ELSEVIER

International Journal of Refrigeration 22 (1999) 354–364

REVUE INTERNATIONALE DU FROID
INTERNATIONAL JOURNAL OF
refrigeration

A 1-D analysis of ejector performance

B.J. Huang*, J.M. Chang, C.P. Wang, V.A. Petrenko

Department of Mechanical Engineering, National Taiwan University, Taipei 106, Taiwan

Received 4 May 1998; received in revised form 25 November 1998; accepted 23 December 1998

Abstract

A 1-D analysis for the prediction of ejector performance at critical-mode operation is carried out in the present study. Constant-pressure mixing is assumed to occur inside the constant-area section of the ejector and the entrained flow at choking condition is analyzed. We also carried out an experiment using 11 ejectors and R141b as the working fluid to verify the analytical results. The test results are used to determine the coefficients, η_p, η_s, ϕ_p and ϕ_m defined in the 1-D model by matching the test data with the analytical results. It is shown that the1-D analysis using the empirical coefficients can accurately predict the performance of the ejectors. © 1999 Elsevier Science Ltd and IIR. All rights reserved.

Keywords: Refrigerating system; Ejector system; Refrigerant; R141b; Ejector; Performance

Analyse unidimensionnelle de la performance d'un éjecteur

Résumé

Dans cette étude, on a effectué une analyse unidimensionnelle pour prédire la performance d'un éjecteur fonctionnant en mode critique. Les auteurs sont partis du principe que le mélange s'effectue à pression constante dans la partie de l'éjecteur dont la section est constante et ont analysé le flux entraîné au niveau de l'onde de choc. Onze éjecteurs utilisant le R141b comme fluide actif ont été utilisés par les auteurs afin de vérifier les résultats analytiques. Les résultats expérimentaux sont utilisés pour déterminer les coefficients η_p, η_s, ϕ_p et ϕ_m définis dans le modèle unidimensionnel. L'étude a montré que l'analyse unidimensionnelle utilisant les coefficients empiriques peut prédire la performance des éjecteurs de façon précise. © 1999 Elsevier Science Ltd and IIR. All rights reserved.

Mots clés: Système frigorifique; Système à éjecteur; Frigorigène; R141b; Éjecteur; Performance

Nomenclature

A	area, m^2
a	sonic velocity, m/s
C_p	specific heat of gas at constant pressure, kJ kg^{-1} K^{-1}
C_v	specific heat of gas at constant volume, kJ kg^{-1} K^{-1}
d	diameter, m
h	enthalpy, kJ kg^{-1}
$\dot{m}$	mass flowrate, kg s^{-1}
M	Mach number
P_c^*	critical back pressure of the ejector, MPa
P_e	vapor pressure at the suction port of the ejector, MPa
P_g	vapor pressure at the nozzle inlet of the ejector, MPa
R	gas constant, kJ kg^{-1} K^{-1}
T	temperature, K
T_c*	saturated-vapor temperature corresponding to the critical back pressure P_c*, K

* Corresponding author. Tel.: + 886-2-2363-4790; fax: + 886-2-2364-0549.

E-mail address: bjhuang@tpts6.seed.net.tw (B.J. Huang)

PII: S0140-7007(99)00004-3

T_e vapor temperature at the suction port of the ejector, K
T_g vapor temperature at the nozzle inlet of the ejector, K
T_{gs} saturated-vapor temperature corresponding to P_g, K
V gas velocity, m s^{-1}
x nozzle position, m
y position of the hypothetical throat
γ $= C_p/C_V$

Superscripts
* critical mode operation of ejector

Subscripts
c exit of ejector; condenser
co limiting condition of ejector operational mode
e inlet port of the entrained flow; hypothetical throat
g nozzle inlet
m mixed flow
p primary flow
p1 nozzle exit
py primary flow at the location of choking for the entrained flow
s suction or entrained flow
sy entrained flow at the location of choking for the entrained flow
t nozzle throat
y location of choking for the entrained flow
1 nozzle exit
2 entrance of the constant-area section
3 exit of the constant-area section

1. Introduction

Ejector air-conditioning or refrigeration system powered by low-grade energy has been studied since the mid-1950s. For utilizing solar or waste heat energy as the heat source, many researchers used refrigerant such as R11, R12, R123, R22, R113, R114, R142, or R142b as the working fluid [1,2]. The performance of refrigerant ejector cooling system is however relatively low as compared to the conventional system. The key problem is in the ejector design.

The ejector design can be classified into two categories according to the position of the nozzle [2]. For the nozzle with its exit located within the constant-area section of an ejector, the mixing of the primary and the entrained flows occurs inside the constant-area section and the ejector is known as "constant-area mixing ejector". For the nozzle with its exit located within the suction chamber which is in front of the constant-area section, the ejector is referred as "constant-pressure mixing ejector". For this kind of ejector, it was assumed that the mixing of the primary and the entrained streams occurs in the suction chamber with a uniform or constant pressure. It is known that the constant-pressure ejector has a better performance than the constant-area ejector and is thus widely used. Therefore, we focus on the design of a "constant-pressure ejector" in the present study, but with a new concept that the mixing occurs within the constant-area section.

The constant-pressure mixing theory of ejector developed by Keenan et al. [3] was frequently used in the analysis of constant-pressure ejector [1,4,5]. Keenan et al. [3] assumed that the pressures of the primary and the entrained flows at the exit of the nozzle have an identical pressure. Mixing of the two streams begins there with a uniform pressure, i.e. constant pressure, until the inlet of the constant-area section.

In practice, two choking phenomena exist in the ejector performance [6,7]: one in the primary flow through the nozzle and the other in the entrained flow. In addition to the choking in the nozzle, the second choking of an ejector results from the acceleration of the entrained flow from a stagnant state at the suction port to a supersonic flow in the constant-area section. Fig. 1 shows the variation of entrainment ratio ω with the discharge or back pressure P_c at fixed suction pressure P_e and fixed primary flow pressure P_g. The ejector performance can then be divided into three operational modes, according to the back pressure P_c:

1. double-choking or critical mode as $P_c \leq P_c{}^*$, while the primary and the entrained flows are both choking and the entrainment ratio is constant, i.e. $\omega =$ constant;
2. single-choking or subcritical mode as $P_c{}^* < P_c < P_{co}$, while only the primary flow is choked and ω changes with the back pressure P_c; and
3. back-flow or malfunction mode as $P_c \geq P_{co}$, while both the primary and the secondary flow are not choked and the entrained flow is reversed (malfunction), i.e. $\omega \leq 0$.

The ejector had better perform at critical mode in order to obtain a better efficiency.

The 1-D constant-pressure mixing theory of Keenan et al. [3] is however unable to analyze the choking of the entrained flow at critical operation mode. In the present study, we developed an 1-D model for the analysis of ejector performance at the critical-mode operation. The constant-

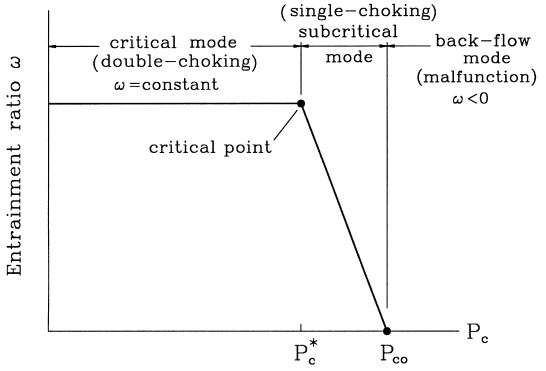

Fig. 1. Operational modes of ejector.

Fig. 1. Modes de fonctionnement de l'éjecteur.

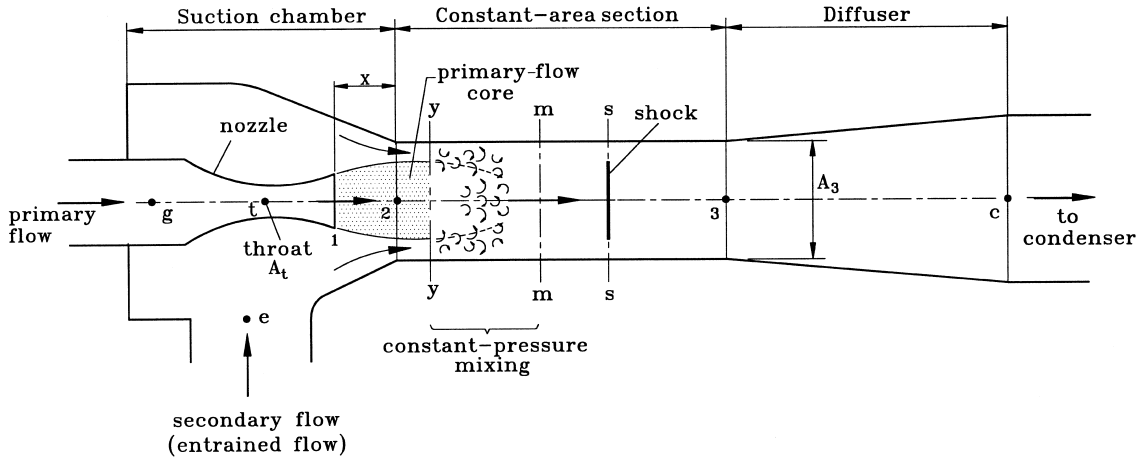

Fig. 2. Schematic diagram of ejector performance.

Fig. 2. Schéma du fonctionnement de l'éjecteur.

pressure mixing is assumed to occur inside the constant-area section and the choking of the entrained flow is predicted. We then carried out an experiment to compare the analytical and test results using various ejectors and R141b as the working fluid.

2. Ejector performance analysis

Keenan et al. [3] assumed that mixing of the two streams takes place inside the suction chamber with a constant or uniform pressure from the exit of the nozzle to the inlet of the constant-area section. Munday and Bagster [6] postulated that after exhausting from the nozzle, the primary flow fans out without mixing with the entrained flow and induces a converging duct for the entrained flow. This duct acts as a converging nozzle such that the entrained flow is accelerated to a sonic velocity at some place, i.e. hypothetical throat. After that, mixing of the two streams starts with a uniform pressure. A hypothetical throat area, or "effective area A_e" [6,7], was defined for the entrained flow at critical operation mode. Huang et al. [7] further determined experimentally the hypothetical throat area A_e for R113 ejector.

In the present study, we assume that the hypothetical throat occurs inside the constant-area section of the ejector. Thus, the mixing of two streams occurs inside the constant-area section with a uniform pressure. Fig. 2 is a schematic diagram showing the mixing process of the two streams in the ejector.

The following assumptions are made for the analysis:

1. The working fluid is an ideal gas with constant properties C_p and γ.
2. The flow inside the ejector is steady and one dimension.
3. The kinetic energy at the inlets of primary and suction ports and the exit of diffuser are negligible.
4. For simplicity in deriving the 1-D model, the isentropic relations are used as an approximation. But to account for non-ideal process, the effects of frictional and mixing losses are taken into account by using some coefficients introduced in the isentropic relations. These coefficients are related to the isentropic efficiency and needs to be determined experimentally.
5. After exhausting from the nozzle, the primary flow fans out without mixing with the entrained flow until at some cross section y–y (hypothetical throat) which is inside the constant-area section.
6. The two streams starts to mix at the cross section y–y (hypothetical throat) with an uniform pressure, i.e. $P_{py} = P_{sy}$, before the shock which is at the cross section s–s.
7. The entrained flow is choked at the cross section y–y (hypothetical throat).
8. The inner wall of the ejector is adiabatic.

2.1. Governing equations

2.1.1. Primary flow through nozzle

For a given inlet stagnant pressure P_g and temperature T_g, the mass flow through the nozzle at choking condition follows the gas dynamic equation:

$$\dot{m}_p = \frac{P_g A_t}{\sqrt{T_g}} \times \sqrt{\frac{\gamma}{R}\left(\frac{2}{\gamma+1}\right)^{(\gamma+1)/(\gamma-1)}} \sqrt{\eta_p}, \tag{1}$$

where η_p is a coefficient relating to the isentropic efficiency of the compressible flow in the nozzle. The gas dynamic relations between the Mach number at the exit of nozzle M_{p1} and the exit cross section area A_{p1} and pressure P_{p1} are, using isentropic relations as an

approximation,

$$\left(\frac{A_{p1}}{A_t}\right)^2 \approx \frac{1}{M_{p1}^2}\left[\frac{2}{\gamma+1}\left(1+\frac{(\gamma-1)}{2}M_{p1}^2\right)\right]^{(\gamma+1)/(\gamma-1)}, \quad (2)$$

$$\frac{P_g}{P_{p1}} \approx \left(1+\frac{(\gamma-1)}{2}M_{p1}^2\right)^{\gamma/(\gamma-1)}. \quad (3)$$

2.1.2. Primary-flow core (from section 1–1 to section y–y)

The Mach number M_{py} of the primary flow at the y–y section follows the isentropic relations as an approximation:

$$\frac{P_{py}}{P_{p1}} \approx \frac{\left(1+((\gamma-1)/2)M_{p1}^2\right)^{\gamma/(\gamma-1)}}{\left(1+((\gamma-1)/2)M_{py}^2\right)^{\gamma/(\gamma-1)}}. \quad (4)$$

For the calculation of the area of the primary flow core at the y–y section, we use the following isentropic relation, but an arbitrary coefficient ϕ_p is included to account for the loss of the primary flow from section 1–1 to y–y:

$$\frac{A_{py}}{A_{p1}} = \frac{(\phi_p/M_{py})\left[(2/(\gamma+1))\left(1+((\gamma-1)/2)M_{py}^2\right)\right]^{(\gamma+1)/(2(\gamma-1))}}{(1/M_{p1})\left[(2/(\gamma+1))\left(1+((\gamma-1)/2)M_{p1}^2\right)\right]^{(\gamma+1)/(2(\gamma-1))}}. \quad (5)$$

The loss may result from the slipping or viscous effect of the primary and the entrained flows at the boundary. The loss actually reflects in the reduction of throat area A_{py} at y–y section through the introduction of the coefficient ϕ_p in Eq. (5).

2.1.3. Entrained flow from inlet to section y–y

From assumption (6), the entrained flow reaches choking condition at the y–y section, i.e. $M_{sy} = 1$. For a given inlet stagnant pressure P_e, we have

$$\frac{P_e}{P_{sy}} \approx \left(1+\frac{\gamma-1}{2}M_{sy}^2\right)^{\gamma/(\gamma-1)}. \quad (6)$$

The entrained flow rate at choking condition follows

$$\dot{m}_s = \frac{P_e \times A_{sy}}{\sqrt{T_e}}\sqrt{\frac{\gamma}{R}\left(\frac{2}{\gamma+1}\right)^{(\gamma+1)/(\gamma-1)}}\sqrt{\eta_s}, \quad (7)$$

where η_s is the coefficient related to the isentropic efficiency of the entrained flow.

2.1.4. Cross-sectional area at section y–y

The geometrical cross-sectional area at section y–y is A_3 that is the sum of the areas for the primary flow A_{py} and for the entrained flow A_{sy}. That is,

$$A_{py} + A_{sy} = A_3. \quad (8)$$

2.1.5. Temperature and Mach number at section y–y

The temperature and the Mach number of the two stream at section y–y follows

$$\frac{T_g}{T_{py}} = 1+\frac{\gamma-1}{2}M_{py}^2, \quad (9)$$

$$\frac{T_e}{T_{sy}} = 1+\frac{\gamma-1}{2}M_{sy}^2. \quad (10)$$

2.1.6. Mixed flow at section m–m before the shock

Two streams starts to mix from section y–y. A shock then takes place with a sharp pressure rise at section s–s. A momentum balance relation thus can be derived as

$$\phi_m\left[\dot{m}_p V_{py} + \dot{m}_s V_{sy}\right] = (\dot{m}_p + \dot{m}_s)V_m, \quad (11)$$

where V_m is the velocity of the mixed flow and ϕ_m is the coefficient accounting for the frictional loss [8]. Similarly, an energy balance relation can be derived as

$$\dot{m}_p\left(C_p T_{py} + \frac{V_{py}^2}{2}\right) + \dot{m}_s\left(C_p T_{sy} + \frac{V_{sy}^2}{2}\right) = (\dot{m}_p + \dot{m}_s)\left(C_p T_m + \frac{V_m^2}{2}\right), \quad (12)$$

where V_{py} and V_{sy} are the gas velocities of the primary and entrained flow at the section y–y:

$$V_{py} = M_{py} \times a_{py}; \qquad a_{py} = \sqrt{\gamma R T_{py}}, \quad (13)$$

$$V_{sy} = M_{sy} \times a_{sy}; \qquad a_{sy} = \sqrt{\gamma R T_{sy}}. \quad (14)$$

The Mach number of the mixed flow can be evaluated using the following relation:

$$M_m = \frac{V_m}{a_m}; \qquad a_m = \sqrt{\gamma R T_m}. \quad (15)$$

2.1.7. Mixed flow across the shock from section m–m to section 3–3

A supersonic shock will take place at section s–s with a sharp pressure rise. Assuming that the mixed flow after the shock undergoing an isentropic process, the mixed flow between section m–m and section 3–3 inside the constant-area section has a uniform pressure P_3. Therefore, the following gas dynamic relations exist:

$$\frac{P_3}{P_m} = 1+\frac{2\gamma}{\gamma+1}(M_m^2-1), \quad (16)$$

$$M_3^2 = \frac{1+((\gamma-1)/2)M_m^2}{\gamma M_m^2 - ((\gamma-1)/2)}. \quad (17)$$

2.1.8. Mixed flow through diffuser

The pressure at the exit of the diffuser follows the

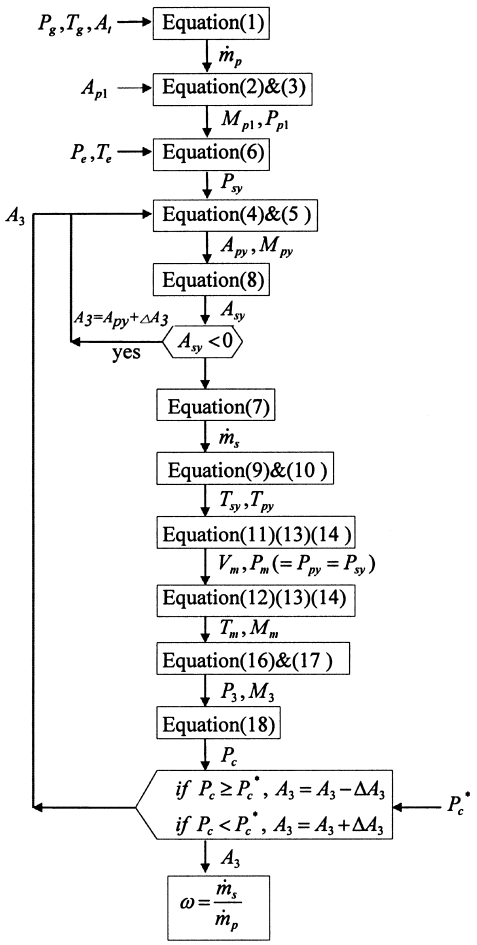

Fig. 3. Simulation flowchart in the ejector performance analysis.

Fig. 3. Diagramme d'analyse pour la simulation de la performance de l'éjecteur.

relation, assuming isentropic process

$$\frac{P_c}{P_3} = \left(1 + \frac{\gamma - 1}{2} M_3^2\right)^{\gamma/(\gamma-1)}. \quad (18)$$

2.2. Ejector performance analysis procedure

Using the above 1-D model of ejector, we can carry out the performance analysis to determine the entrainment ratio ω and the required cross sectional area of the constant-area section A_3. For a given nozzle throat area A_t (or diameter d_t) and nozzle exit area A_{p1} (or diameter d_{p1}), the performance of an ejector is characterized by the stagnant temperature and pressure at the nozzle inlet (T_g, P_g) and at the suction inlet port (T_e, P_e), the critical back pressure P_c*. That is, there are 5 independent variables (T_g, P_g, T_e, P_e, P_c*) in the ejector performance analysis. The analysis procedure follows the flowchart shown in Fig. 3. The output of the analysis includes the primary flow $\dot{m}_p$, the entrained flow $\dot{m}_s$, the entrainment ratio ω, the cross sectional area of the constant-area section A_3 and the area ratio A_3/A_t.

3. Experimental verification

3.1. Experimental setup

Fig. 4 shows the schematic diagram of the test facility. R141b is selected as the working fluid in the present study as R141b has a positive-slope saturated-vapor line in the thermodynamic T–s diagram [9]. This will not produce a condensation for the vapor expansion in the ejector and thus reduces losses.

The design and operation of the test facility is the same as that described in the previous article [10]. It takes about 1 h to warm up the test facility and about 30 min for each steady-state test run.

3.2. Ejector specifications

To verify the theoretical analysis using the present model, we have tested 11 different ejectors. The ejector is designed in three major parts: nozzle, suction chamber body, and constant-area section (including diffuser). The standard connections between the different parts are used so that all the parts are interchangeable. Two nozzles (A, E) are designed and fabricated in the experiment. The specifications of the nozzles are listed in Table 1. We designed 8 different constant-area sections (including diffuser) as listed in Table 2. Eleven ejectors are used in the present experiment. The area ratio A_3/A_t of the tested ejectors ranges from 6.44 to 10.64.

3.3. Comparison of analysis with test results

The 11 ejectors were tested under various operating conditions. For easy understanding, we also present the saturated vapor temperatures in the parenthesis for the pressures

Table 1
Nozzle design

Tableau 1
Caractéristiques des tuyères

Nozzle	Throat diameter, d_t (mm)	Exit diameter, d_{pl} (mm)	A_{pl}/A_t
A	2.64	4.50	2.905
E	2.82	5.10	3.271

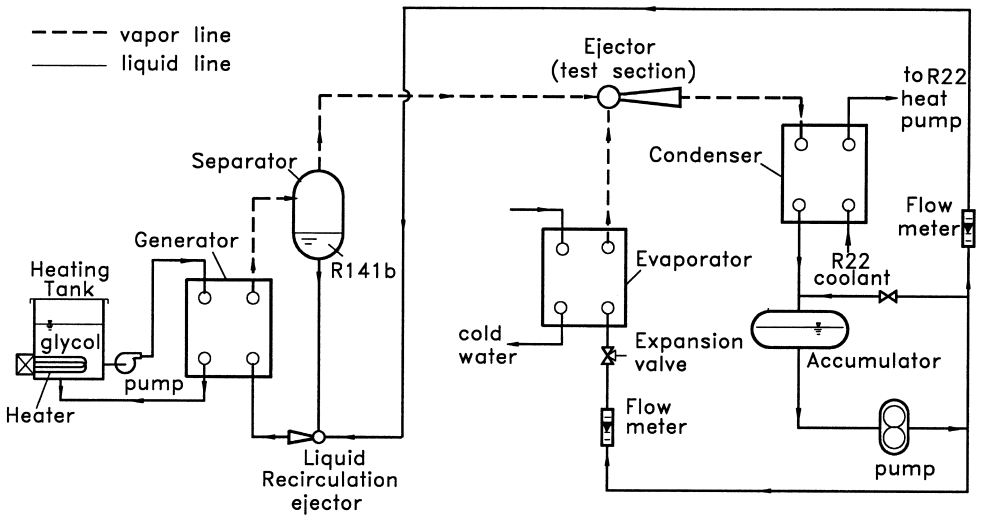

Fig. 4. Schematic diagram of the ejector test facility.

Fig. 4. Schéma du dispositif utilisé pour tester les éjecteurs.

shown in the figures. That is, T_c* represents the saturated vapor temperature of the critical back pressure P_c*. T_{gs} represents the saturated vapor temperature of the primary flow pressure at the inlet of the nozzle P_g.

For abbreviation, ejector AB represents the ejector assembly of nozzle A and constant-area section B, for example.

Shown in Tables 3 and 4 are the theoretical calculations of the required ejector area ratio A_3/A_t and the critical-mode entrainment ratio ω at various operating conditions. For the ejectors having a A_3/A_t consistent with the calculated (or required) value to within $\pm$ 10% deviation (as shown in Figs. 5 and 6), the measured ω coincide fairly well with the calculated results using the present 1-D analysis, mostly within $\pm$ 15% error, as can be seen from Figs. 7 and 8.

As all the ejectors were performed at critical mode, only the critical-point performance is shown and discussed in the present study.

In the 1-D analysis, the coefficients accounting for the loss in the primary flow in the nozzle and in the suction flow before mixing are taken as $\eta_p = 0.95$ and $\eta_s = 0.85$, respectively. They are not very sensitive to the analytical results as the values adopted approximate that for isentropic process. The coefficient of the primary flow leaving the nozzle is taken as $\phi_p = 0.88$. It was found that the loss coefficient ϕ_m in Eq.(11) is more sensitive than the other coefficients and should be taken to vary slightly with the ejector area ratio A_3/A_t in order to fit the test results. An empirical relation is found

$$\phi_m = \begin{cases} 0.80, & \text{for } A_3/A_t > 8.3, \\ 0.82, & \text{for } \leq A_3/A_t \leq 8.3, \\ 0.84, & \text{for } A_3/A_t \leq 6.9. \end{cases} \quad (19)$$

Fig. 9 shows the variations of the ejector area ratio with

Table 2
Constant-area section design and ejector specification ((XX): ejector model)

Tableau 2
Caractéristiques de la partie à section constante et de l'éjecteur [(XX): modèle d'éjecteur]

Constant-area section			Ejector specification			
Serial No.	d_3 (mm)	Inlet converging angle, (°)	A_3/A_t (with Nozzle A)		A_3/A_t (with Nozzle E)	
A	6.70	68	6.44	(AA)		
B	6.98	60	6.99	(AB)		
G	7.34	60	7.73	(AG)	6.77	(EG)
C	7.60	67	8.29	(AC)	7.26	(EC)
D	8.10	68	9.41	(AD)	8.25	(ED)
E	8.54	67			9.17	(EE)
F	8.84	67			9.83	(EF)
H	9.20	62			10.64	(EH)

Table 3
Comparisons of test and analytical results at $P_e = 0.040$ MPa (8°C) ((XX): ejector specification; error = (theory − experiment)/experiment)

Tableau 3
Comparaison des résultats expérimentaux et analytiques où $P_e = 0{,}040$ MPa (8°C) [(XX): modèle d'éjecteur; erreur (théorique − expérimentale)/(expérimentale)]

P_g, Mpa (T_{gs}, °C)	T_c* (°C)	A_3/A_t			ω		
		Theory	Experiment	Error, %	Theory	Experiment	Error, %
0.604	31.3	10.87	10.64 (EH)	2.10	0.4627	0.4377	5.70
(95)	33.0	9.67	9.83 (EF)	− 1.62	0.3774	0.3937	− 4.13
	33.6	9.29	9.41 (AD)	− 1.32	0.3476	0.3457	0.56
	34.2	8.89	9.17 (EE)	− 3.02	0.3253	0.3505	− 7.20
	36.3	8.57	8.28 (AC)	3.43	0.2983	0.2814	6.01
	37.1	8.12	8.25 (ED)	− 1.63	0.2658	0.2902	− 8.39
	38.8	7.27	7.26 (EC)	0.14	0.2078	0.2273	− 8.57
	38.6	7.38	7.73 (AG)	− 4.51	0.2144	0.2552	− 15.98
	41.0	7.05	6.77 (EG)	4.00	0.1919	0.2043	− 6.06
	42.1	6.55	6.44 (AA)	1.65	0.1554	0.1859	− 16.43
0.538	31.5	9.28	9.41 (AD)	− 1.39	0.4178	0.4446	− 6.02
(90)	33.8	8.53	8.28 (AC)	2.94	0.3552	0.3488	1.84
	36.7	7.03	7.73 (AG)	− 9.03	0.2395	0.3040	− 21.22
	37.5	6.65	6.99 (AB)	− 4.86	0.2093	0.2718	− 22.99
	38.9	6.74	6.44 (AA)	4.66	0.2156	0.2246	− 3.99
0.465	28.0	9.34	9.41 (AD)	− 0.73	0.5215	0.5387	− 3.19
(84)	30.5	8.68	8.28 (AC)	4.71	0.4605	0.4241	8.58
	32.3	7.68	7.73 (AG)	− 0.62	0.3704	0.3883	− 4.61
	33.6	6.99	6.99 (AB)	0.00	0.3042	0.3117	− 2.39
	35.5	6.79	6.44 (AA)	5.35	0.2880	0.2880	0.23
0.400	24.4	9.92	9.41 (AD)	5.41	0.6944	0.6227	11.51
(78)	26.9	8.97	8.28 (AC)	8.23	0.5966	0.4889	22.03
	29.1	7.64	7.73 (AG)	− 1.17	0.4609	0.4393	4.93
	29.5	7.48	6.99 (AB)	7.03	0.4422	0.3922	12.74
	32.5	6.62	6.44 (AA)	2.78	0.3525	0.3257	8.24

Table 4
Comparisons of test and analytical results at $P_e = 0.047$ MPa (12°C) ((XX): ejector specification; error = (theory − experiment)/experiment)

Tableau 4
Comparaison des résultats expérimentaux et analytiques où $P_e = 0{,}047$ MPa (12°C) [(XX): modèle d'éjecteur; erreur = (théorique − expérimentale)/(expérimentale)]

P_g, Mpa (T_{gs}, °C)	T_c* (°C)	A_3/A_t			ω		
		Theory	Experiment	Error, %	Theory	Experiment	Error, %
0.604	33.1	10.43	9.83 (EF)	6.16	0.5482	0.4989	9.89
(95)	34.2	9.67	9.17 (EE)	5.45	0.4894	0.4048	10.55
	34.5	9.47	9.41 (AD)	0.63	0.4708	0.4541	3.67
	38.7	7.96	7.73 (AG)	2.95	0.3434	0.3503	− 1.97
	39.3	7.69	7.26 (EC)	5.92	0.3235	0.3040	6.41
	42.5	6.91	6.44 (AA)	7.33	0.2573	0.2350	9.49
0.538	32.0	9.50	9.41 (AD)	0.91	0.5573	0.5422	2.78
(90)	36.0	8.00	7.73 (AG)	3.49	0.4142	0.4034	2.67
	39.5	7.03	6.44 (AA)	9.17	0.3257	0.2946	10.54
0.465	28.9	9.63	9.41 (AD)	2.28	0.6906	0.6350	8.75
(84)	32.4	8.17	7.73 (AG)	5.67	0.4769	0.4790	12.09
	36.0	7.07	6.44 (AA)	9.78	0.4147	0.3398	22.04
0.400	25.7	9.85	9.41 (AD)	4.60	0.8626	0.7412	16.37
(78)	29.2	8.26	7.73 (AG)	6.89	0.6659	0.6132	8.60

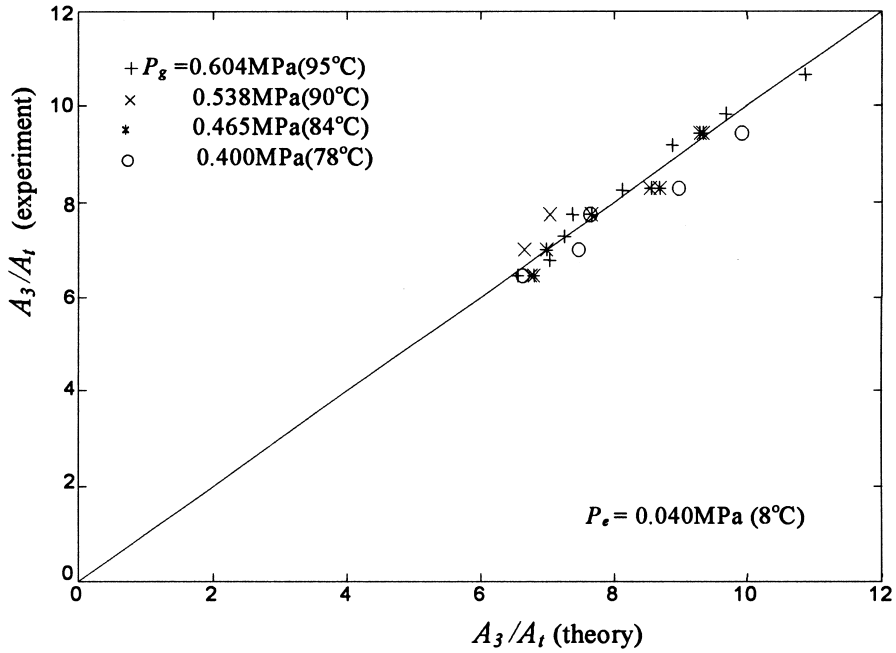

Fig. 5. Comparison between the theoretical calculation and the experimental design of the ejector area ratio at P_e = 0.040 MPa (8°C).

Fig. 5. Comparaison entre les valeurs calculée et expérimentale du rapport des surfaces de l'éjecteur pour P_e = 0,040 MPa (8°C).

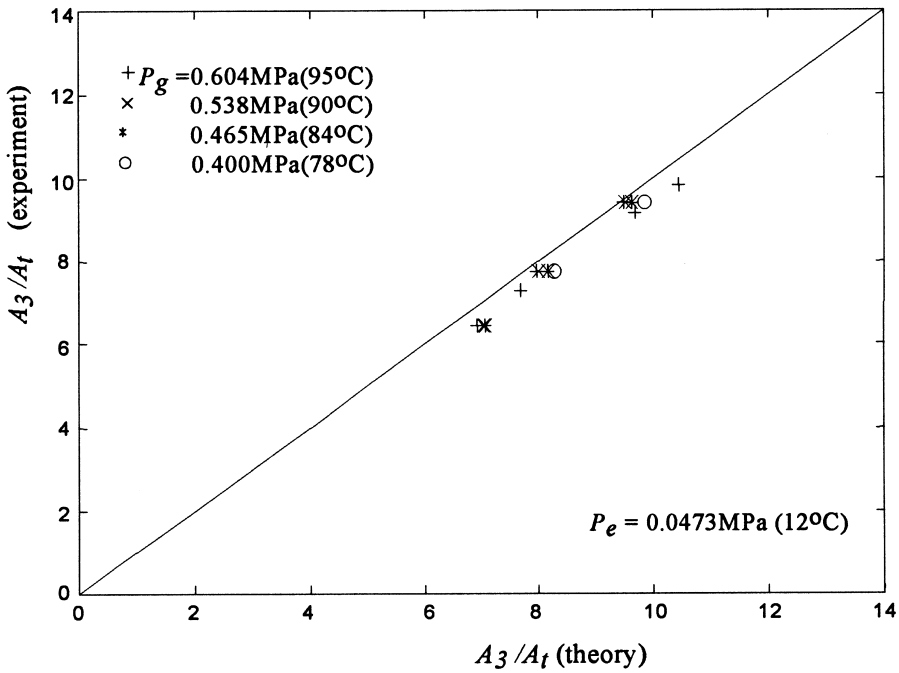

Fig. 6. Comparison between the theoretical calculation and the experimental design of the ejector area ratio at P_e = 0.047 MPa (12°C).

Fig. 6. Comparaison entre les valeurs calculée et expérimentale du rapport de la superficie de l'éjecteur pour P_e = 0,047 MPa (12°C).

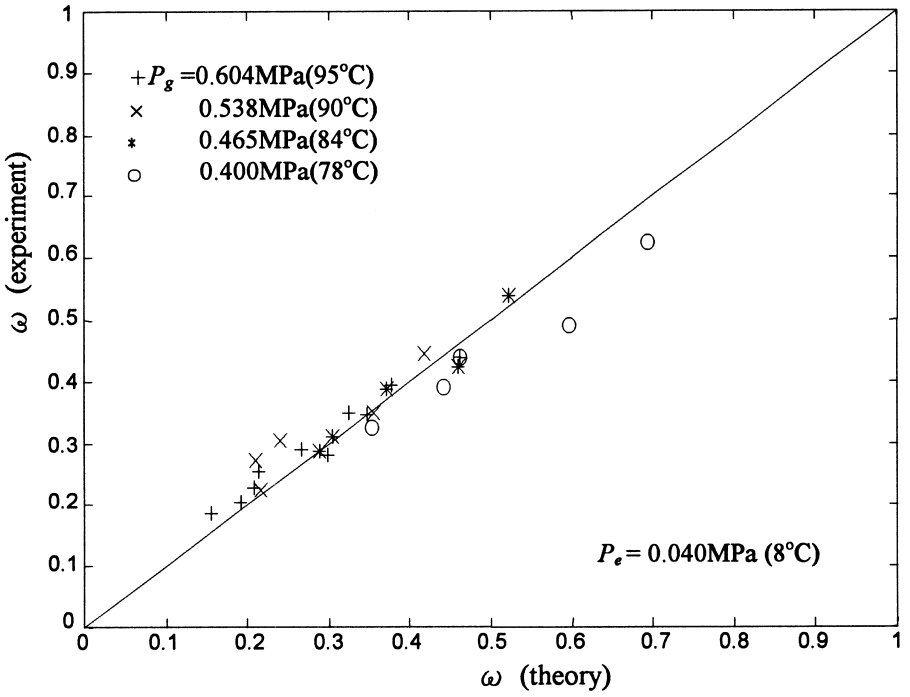

Fig. 7. Comparison between the theoretical calculation and the experimental design of the ejector entrainment ratio at $P_e = 0.040$ MPa (8°C).

Fig. 7. Comparaison entre les valeurs calculée et expérimentale du rapport de l'entraînement de l'éjecteur pour $P_e = 0{,}040$ MPa (8°C).

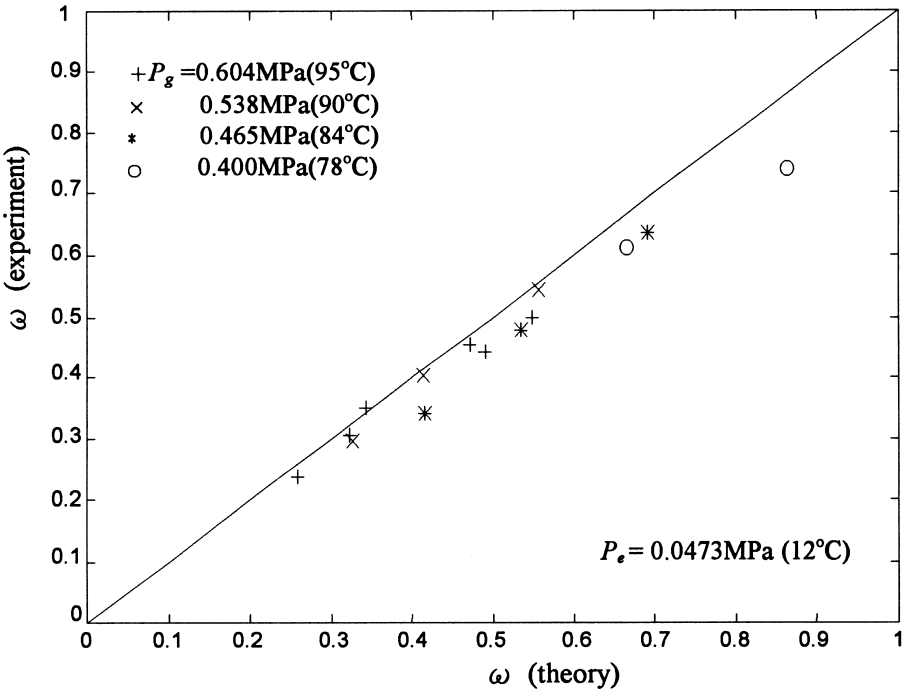

Fig. 8. Comparison between the theoretical calculation and the experimental design of the ejector entrainment ratio at $P_e = 0.047$ MPa (12°C).

Fig. 8. Comparaison entre les valeurs calculée et expérimentale du rapport de l'entraînement de l'éjecteur pour $P_e = 0{,}047$ MPa (12°C).

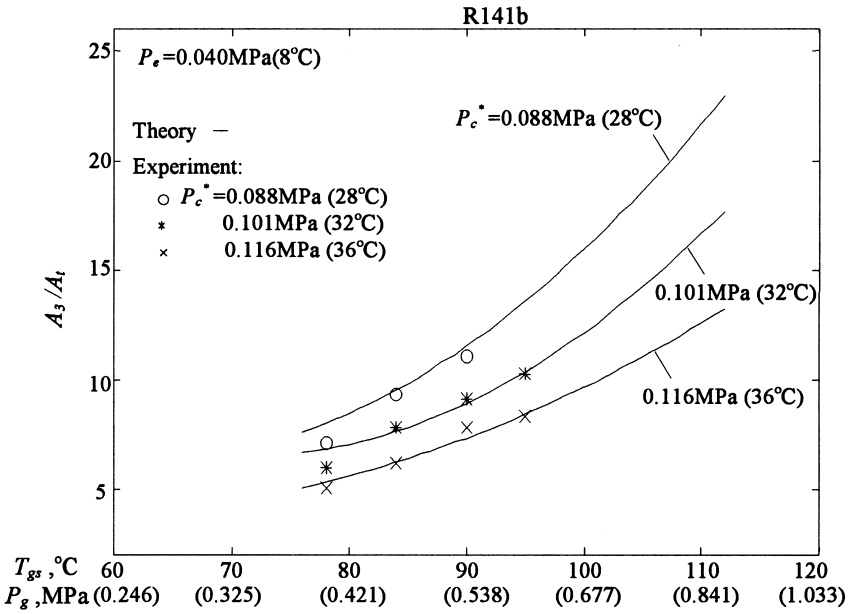

Fig. 9. Variation of ejector area ratio with the vapor pressure at the nozzle inlet.

Fig. 9. Variation du rapport des surfaces de l'éjecteur en fonction de la pression à l'entrée de la tuyère.

the primary flow pressure and its saturated temperature at the inlet of the nozzle. The theoretical or required A_3/A_t is seen to increase with increasing primary flow inlet pressure P_g for a fixed ejector critical back pressure P_c*. A_3/A_t of an ejector also increases with decreasing P_c* for a fixed P_g.

Fig. 10 shows that the measured ω coincide with the analysis. The theoretical calculations also show that the entrainment ratio can be further improved by raising the primary flow pressure with a matching ejector having higher A_3/A_t. For R141b, it is seen that ω can reach 0.7

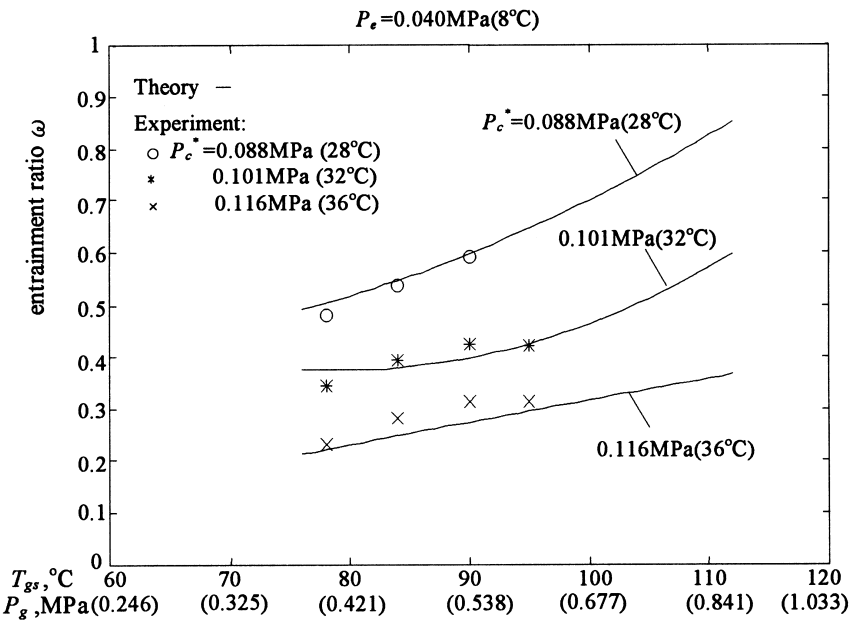

Fig. 10. Variation of ejector entrainment ratio with the vapor pressure at the nozzle inlet.

Fig. 10. Variation du rapport d'entraînement de l'éjecteur en fonction de la pression à l'entrée de la tuyère.

at $P_g = 0.677$ MPa ($T_{gs} = 100$°C) for an ejector having a $A_3/A_t \approx 16.0$.

4. Discussion

In the 1-D analysis, we need to know the coefficients η_p, η_s, ϕ_p, and ϕ_m which account for various losses in ejector. These values are related to the ejector design and manufacturing technique. They depend on machining, center-line alignment, interior surface polishing, material used and suction port configuration etc. The determination of these coefficients relies on experiences. The test results are used to determine the coefficients η_p, η_s, ϕ_p, and ϕ_m defined in the 1-D model by matching the test data with the analytical results. The present 1-D analysis thus can be treated as semi-empirical from this viewpoint.

Bases on the experimental results obtained from the 11 ejectors with good quality in machining, it is satisfactory to take $\eta_p = 0.95$, $\eta_s = 0.85$ and $\phi_p = 0.88$. The loss coefficient ϕ_m was found to vary slightly with the ejector area ratio A_3/A_t and follows Eq. (19). However, a more convenient but rough relation can also be used:

$$\phi_m = 1.037 - 0.02857\frac{A_3}{A_t}. \quad (20)$$

The nozzle position is also an important factor affecting the ejector performance [11]. In the present study, the distance of the nozzle exit measured from the inlet of the constant-area section X is adjusted such that the ejector obtains the best performance at each operating condition. It is found experimentally that the ratio X/d_3 is around 1.50 for the best ejector performance and the test results obtained are used to compare with the analysis.

The degree of superheating of the primary and entrained flows before entering the ejector is another factor that may affect the performance. In the present study, we used no superheating in the primary flow.

The superheating of the entrained flow is in the range of 5–20 K in the present experiment. We found that the ejector performance will not vary with the degree of superheating of the entrained flow in this range. This means that the present results are valid for the ejector with the degree of superheating exceeding 5 K in the entrained flow. The need in the superheating depends on the particular thermodynamic properties of the working fluid. For working fluid with a negative-slope saturated-vapor line in the thermodynamic T–s diagram (i.e. bell-shaped saturation line), an isentropic expansion of the vapor would possibly induce a condensation that will seriously affect the gas dynamic process in the ejector and the performance of the ejector as well. The working fluid R141b used in the present study has a positive-slope saturated-vapor line in the thermodynamic T–s diagram [9]. Therefore, superheating is not as important as other working fluids.

5. Conclusion

In the present study, we carried out a 1-D analysis for the prediction of the ejector performance at critical-mode operation. The constant-pressure mixing is assumed to occur inside the constant-area section of the ejector and the entrained flow at choking condition is analyzed. We have also carried out an experiment to verify the analytical results using 11 ejectors and R141b as the working fluid. The test results are used to determine the coefficients η_p, η_s, ϕ_p, and ϕ_m defined in the 1-D model by matching the test data with the analytical results. It is shown that the1-D analysis using the empirical coefficients can accurately predict the performance of the ejectors.

Acknowledgements

The present study was supported by the National Science Council, ROC, Taiwan, through Grant No.NSC86-2811-E-002-004R.

References

[1] Sun D-W, Emes IW. Performance characteristics of HCFC-123 ejector refrigeration cycles. Int. J. Energy Res. 1996;20:871–885.
[2] Sun D-W. Recent developments in the design theories and applications of ejectors—a review. J. Inst. Energy 1995;68:65–79.
[3] Keenan H, Neumann EP, Lustwerk F. An investigation of ejector design by analysis and experiment. J. Appl. Mech., Trans. ASME 1950;72:299–309.
[4] Sun D-W. Variable geometry ejectors, their applications in ejector refrigeration systems. Energy 1996;21:919–929.
[5] Sun D-W. Experimental investigation of the performance characteristics of a steam jet refrigeration system. Energy Sources 1997;19:349–367.
[6] Munday, John T, Bagster DF. A new ejector theory applied to steam jet refrigeration. Ind. Engng Chem., Process Des. Dev. 1977;16:442–449.
[7] Huang BJ, Jiang CB, Fu FL. Ejector performance characteristics and design analysis of jet refrigeration system. ASME J. Engng Gas Turbines and Power 1985;107:792–802.
[8] Eames IW, Aphornratana S, Haider H. A theoretical and experimental study of a small-scale steam jet refrigerator. Int. J. Refrig. 1995;18:378–386.
[9] Morrison G. The shape of the temperature–entropy saturation boundary. Int. J. Refrig. 1994;18:21–30.
[10] Huang BJ, Chang JM. Empirical correlation for ejector design. Int. J. Refrig. 1999;22:379–388.
[11] Aphornratana S, Eames IW. A small capacity steam-ejector refrigerator: experimental investigation of a system using ejector with movable primary nozzle. Int. J. Refrig. 1997;20:352–358.